

Correlation between the boson peak frequency and transverse Ioffe-Regel limit in four-dimensional structural glasses

Licun Fu¹, Xinyu Chang¹, and Lijin Wang^{1,*}

¹School of Physics, State Key Laboratory of Opto-Electronic Information Acquisition and Protection Technology, Anhui University, Hefei 230601, China

* Corresponding author, Email: lijn.wang@ahu.edu.cn

(Dated: December 8, 2025)

The emergence of excess vibrational modes over the Debye prediction, typically manifested as the well-known boson peak in the plot of vibrational density of states scaled by the Debye prediction, has become a hallmark of various amorphous solids. The origin of the boson peak has been attracting considerable attention but is still under debate. A popular view is that the position of the boson peak coincides well with that of the Ioffe-Regel limit for transverse modes in both two- and three-dimensional glasses, which is primarily derived from simulation studies of model structural glasses. However, it remains unknown whether the proposed coincidence could be generalized to higher spatial dimensions, and addressing this could contribute to the advancement of relevant phenomenological theories. Here, we find that the transverse Ioffe-Regel limit frequency is higher than and not proportional to the boson peak frequency in our studied four-dimensional glasses. Our findings therefore suggest that the proposed coincidence between the boson peak frequency and the transverse Ioffe-Regel limit depends on spatial dimensions, which was not anticipated previously.

I. INTRODUCTION

Glasses have long played a pivotal role in the development of human civilization. Nevertheless, the nature of glasses continues to represent one of the most challenging scientific questions [1–3]. Compared to crystalline materials, glasses exhibit distinct low-temperature thermodynamic properties [4–6], particularly in terms of heat capacity and thermal conductivity. One promising approach to understand these thermodynamic properties is to decipher low-frequency vibrational peculiarities of glasses [2, 3, 7–9].

For crystals, the vibrational density of states (VDOS) at low frequencies ω follows the Debye prediction as $D(\omega) = A_D \omega^{d-1}$ in d dimensions with A_D the Debye level [10]. However, the low-frequency VDOS in various glasses has been consistently observed to exceed the Debye prediction [2, 3, 11–18], typically manifested as an apparent peak in the plot of $D(\omega)/\omega^{d-1}$ versus ω . This peak is commonly referred to as the boson peak, and the corresponding frequency is known as the boson peak frequency ω_{BP} . Importantly, the temperature scale corresponding to ω_{BP} was found to be approximately located within the plateau region of thermal conductivity's temperature dependence as well as within the bump in the plot of heat capacity scaled by temperature squared [7]. Therefore, elucidating the nature of vibrational modes in the vicinity of the boson peak may provide valuable insights into the understanding of thermodynamic anomalies. Indeed, this objective represents one of the primary motivations behind numerous studies attempting to elucidate the origin of the boson peak or its correlation with other characteristics [3]. Over the decades, a variety of explanations have been proposed; however, no consensus has yet been reached regarding the origin of the boson peak [19–27].

Due to the inherent disorder and anharmonicity in glasses, phonons—even at extremely low frequencies—experience damping when propagating through glasses, as evidenced by a decreasing mean free path or lifetime of phonons with increasing frequencies [28–38]. When the mean free path of phonons decreases to half their wavelength, the frequency ω_{IR} corresponding to the Ioffe-Regel limit is reached [39, 40]. Therefore, there will be no well-defined phonons any longer at frequencies above ω_{IR} . Moreover, ω_{IR} has been claimed to coincide with the crossover from weak to strong scattering of phonons in glasses [38, 40–42].

Interestingly, over the past two decades, one popular view is that ω_{BP} corresponds to the transverse Ioffe-Regel limit $\omega_{IR,T}$, which was mainly supported by simulation studies of two- (2D) and three-dimensional (3D) structural glasses [19, 38, 43–49]. There are several additional simulation studies observing that ω_{BP} coincides with both transverse and longitudinal ($\omega_{IR,L}$) Ioffe-Regel limits in model vitreous silica glasses [40, 50] and model gels [46], where the equality $\omega_{IR,T} = \omega_{IR,L}$ was followed. Note that the inequality $\omega_{IR,T} < \omega_{IR,L}$ has been observed in most model structural glasses [43, 51]. However, simulation studies [20, 52] of mass-spring networks where specific types of disorder could be tuned artificially, suggest that it's possible to observe the inequality between $\omega_{IR,T}$ and ω_{BP} under appropriate conditions, whereas no such inequality has ever been observed in model structural glasses where multiple types of disorder coexist. Additionally, there appears to be no consensus on the relation between the Ioffe-Regel limit and the boson peak based on experimental observations [53–59].

To the best of our knowledge, nearly all numerical investigations of the correlation between the transverse Ioffe-Regel limit and the boson peak are done in 2D and/or 3D model structural glasses. And these studies

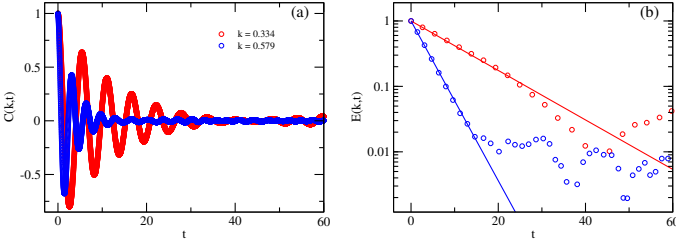


FIG. 1. (a) Illustration of velocity correlation functions $C(k, t)$ at wavevectors $k = 0.334$ and $k = 0.579$ in 4D glasses. (b) Time dependence of the envelope $E(k, t)$ determined by the peaks in the absolute value of $C(k, t)$ shown in (a). Data in (a) and (b) are obtained at $\rho = 0.8$ in 4D IPL-12 glasses.

consistently found $\omega_{\text{IR},T} = \omega_{\text{BP}}$. Then, it is natural to consider what might happen to their relation when moving into higher spatial dimensions, and addressing this is important to the development of relevant phenomenological theories.

In this work, we performed computer simulation studies in four-dimensional (4D) structural glasses. Unexpectedly, we find the equality $\omega_{\text{IR},T} = \omega_{\text{BP}}$ does not hold any more in 4D glasses studied. Specifically, we observe that $\omega_{\text{IR},T} > \omega_{\text{BP}}$, and $\omega_{\text{IR},T}$ is not proportional to ω_{BP} in our studied 4D glasses.

II. SIMULATION DETAILS

We simulated model glass formers with two different types of interaction potentials: (I) The inverse power law potential and (II) the spring-like potential [60]. Each 4D model glass former is composed of a 50:50 binary mixture of A particles and B particles with equal mass (set to one in this work). Specifically, the interaction potential models employed in our 4D simulations are as follows:

(1) The inverse power law (IPL) potential model. In this model, the interaction between two particles i and j is $V(r_{ij}) = [(\frac{\sigma_{ij}}{r_{ij}})^n + c_0 + c_2(\frac{r_{ij}}{\sigma_{ij}})^2 + c_4(\frac{r_{ij}}{\sigma_{ij}})^4]G(r_{ij}^c - r_{ij})$. Here, $G(r)$ is the Heaviside step function, r_{ij} is the particle separation, $\sigma_{AA} = 1.0$, $\sigma_{BB} = 1.4$, and $\sigma_{AB} = 1.18$. The polynomial terms are introduced to smooth $V(r_{ij})$ up to its second derivative at the interaction cutoff $r_{ij}^c = 1.48\sigma_{ij}$. Here, we employed $n = 10$ (hereafter referred to as IPL-n10), and $n = 14$ (IPL-n14).

(2) The spring-like potential model. In this model, $V(r_{ij}) = \frac{1}{\alpha}(1 - \frac{\sigma_{ij}}{r_{ij}})^\alpha G(\sigma_{ij} - r_{ij})$, where $\sigma_{AA} = 1.0$, $\sigma_{BB} = 1.4$, and $\sigma_{AB} = 1.2$. Here, we employed $\alpha = 2$ corresponding to the harmonic potential (hereafter referred to as HARM), and $\alpha = 2.5$ corresponding to the Hertzian potential (HERTZ).

Different 4D model glass formers were created by varying the types of interaction potentials and number densities $\rho = N/L^d$ with L the side length and N the total number of particles. In particular, the system sizes in 4D range from 20000 to 300000, depending on number

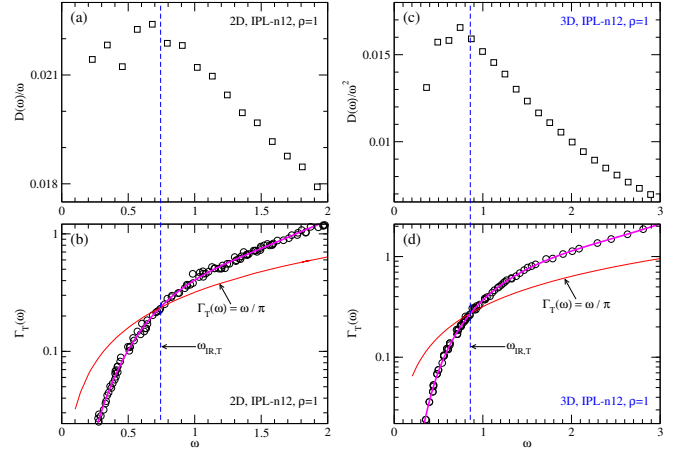


FIG. 2. Reduced VDOS $D(\omega)/\omega$ in (a) and transverse sound attenuation coefficient $\Gamma_T(\omega)$ in (b) at $\rho = 1$ in 2D IPL-12 glasses with N ranging from 20000 to 50000. Reduced VDOS $D(\omega)/\omega^2$ in (c) and transverse sound attenuation coefficient $\Gamma_T(\omega)$ in (d) at $\rho = 1$ in 3D IPL-12 glasses with N ranging from 48000 to 192000. The lines passing through data points of $\Gamma_T(\omega)$ in (b) and (d) are obtained from polynomial fits.

densities and interaction potential models.

To avoid redundancy and potential confusion, we omit here the simulation details for the 2D and 3D data presented in this work, which were obtained from IPL glass models with $n = 12$ (hereafter referred to as IPL-n12). For further details on 2D IPL glass models, readers are referred to Ref. [13]; for 3D IPL glass models, see Ref. [12].

Zero-temperature ($T = 0$) glasses were produced by quenching instantaneously high-temperature liquids to $T = 0$ via energy minimization (here we use the fast inertial relaxation engine [61]). The frequencies of vibrational modes were determined through the diagonalization (using math kernel library [62]) of the dynamic matrix derived from $T = 0$ glasses. The vibrational density of states is given by $D(\omega) = \frac{1}{dN-d} \sum_{l=1}^{dN-d} \delta(\omega - \omega_l)$, where ω_l is the frequency corresponds to the l -th vibrational mode.

The transverse sound attenuation coefficient (or inverse lifetime) $\Gamma_T(\omega)$ was determined as follows. First, the initial velocity of particle i was set to $\dot{\mathbf{u}}_i(t=0) = \mathbf{b} \sin(\mathbf{k} \cdot \mathbf{r}_i)$. Here, $\mathbf{b} \cdot \mathbf{k} = 0$, \mathbf{k} is the wavevector, \mathbf{b} is a unit vector, and \mathbf{r}_i is the position vector of particle i at $t = 0$ in $T = 0$ glasses. Second, we performed molecular dynamics (MD) simulations by solving the equation of motion [30] which reads

$$\ddot{\mathbf{u}}_i(t) = \dot{\mathbf{u}}_i(t=0)\delta(t) - \sum_{j=1}^N D_{ij}\mathbf{u}_j(t), \quad (1)$$

where D_{ij} is the dynamic matrix of $T = 0$ glasses, and $\mathbf{u}_i(t)$ represents the displacement of particle i at t relative to its initial position. During MD simulations, we

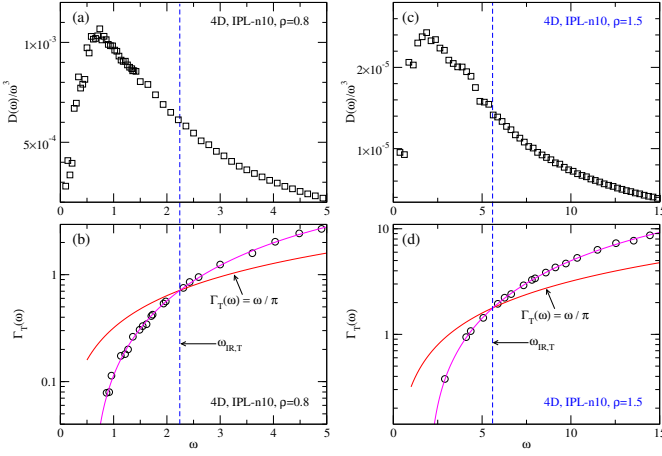


FIG. 3. Reduced VDOS $D(\omega)/\omega^3$ in (a) and (c) and transverse sound attenuation coefficient $\Gamma_T(\omega)$ in (b) and (d) in 4D IPL-10 glasses. Data in (a) and (b) are obtained at $\rho = 0.8$, and (c) and (d) are at $\rho = 1.5$. The lines passing through data points of $\Gamma_T(\omega)$ in (b) and (d) are obtained from polynomial fits.

calculated the velocity correlation function

$$C(k, t) = \left\langle \frac{\sum_{i=1}^N \dot{\mathbf{u}}_i(0) \cdot \dot{\mathbf{u}}_i(t)}{\sum_{i=1}^N \dot{\mathbf{u}}_i(0) \cdot \dot{\mathbf{u}}_i(0)} \right\rangle. \quad (2)$$

The transverse sound attenuation $\Gamma_T(\omega)$ and the corresponding frequency ω could be obtained by fitting the $C(k, t)$ data to

$$C(k, t) = \exp(-\Gamma_T(\omega)t/2) \cos(\omega t). \quad (3)$$

Note that ω depends on k , and so does $\Gamma_T(\omega)$. k in this work ranges approximately from 0.13 to 1.58, and the specific values of k (satisfying periodic boundary conditions) depend on systems examined.

III. RESULTS

Figure 1(a) illustrates the time evolution of $C(k, t)$ calculated at two different k in 4D glasses. One could observe that $C(k, t)$ decays faster at a higher k . In addition, the decay at long time is abnormal, which could be seen more clearly from the time evolution of the envelopes of $C(k, t)$, $E(k, t)$, see Fig. 1(b). Here, $E(k, t)$ corresponds to all peaks in $|C(k, t)|$ and exhibits significant fluctuations at long time scales at each fixed k . Note that such anomalous decay of $E(k, t)$ at long time has been observed as well in both 2D and 3D glass systems, which was demonstrated to be due to finite-size effects [30, 32, 35].

To eliminate the finite-size effects, a restricted envelope fit method has been introduced in recent years to get $\Gamma_T(\omega)$ in simulations in 2D and 3D glasses [32–35].

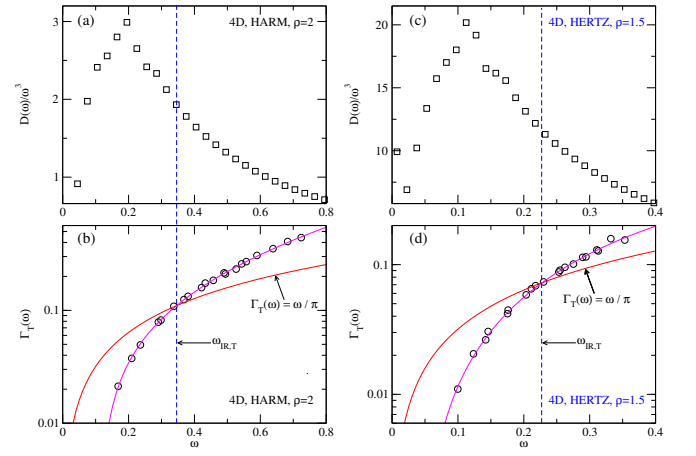


FIG. 4. Reduced VDOS $D(\omega)/\omega^3$ in (a) and (c) and transverse sound attenuation coefficient $\Gamma_T(\omega)$ in (b) and (d) in 4D glasses with spring-like potentials. Data in (a) and (b) are calculated at $\rho = 2$ in HARM glasses, and (c) and (d) are at $\rho = 1.5$ in HERTZ glasses. The lines passing through data points of $\Gamma_T(\omega)$ in (b) and (d) are obtained from polynomial fits.

In this work, we employed the same method to get $\Gamma_T(\omega)$ in 4D glasses. Specifically, as illustrated in Fig. 1(b), the appropriate short-time $E(k, t)$ data are selected to fit to the equation $E(k, t) = \exp(-\Gamma(\omega)t/2)$. We observe that the resulting $\Gamma_T(\omega)$ exhibits no finite-size effects in 4D glasses. Unless otherwise specified, all $\Gamma_T(\omega)$ data presented below are derived from measurements across different system sizes. Additionally, the frequency $\omega_{IR,T}$ corresponding to the transverse Ioffe-Regel limit is determined as the value when $\pi\Gamma_T(\omega) = \omega$ [43].

The investigation of the correlation between the Ioffe-Regel limit and the boson peak has attracted considerable attention. Based on experimental studies [53–58], their correlation remains an unresolved issue that requires further investigations. However, a growing consensus has emerged from simulation studies over the past two decades [19, 38, 40, 43–50]. These simulation studies suggested that the transverse Ioffe-Regel limit coincides with the boson peak frequency, i.e., $\omega_{IR,T} = \omega_{BP}$, irrespective of interaction potentials or spatial dimensions (at least in 2D and 3D). Regarding the relation between $\omega_{IR,T}$ and $\omega_{IR,L}$, it was found $\omega_{IR,T} < \omega_{IR,L}$ in most model structural glasses [43], whereas simulation studies on model silica glasses [40, 50] reported $\omega_{IR,T} = \omega_{IR,L} = \omega_{BP}$, suggesting that both the transverse and longitudinal Ioffe-Regel limits coincide with the boson peak. Despite possible variations in the relative positions of $\omega_{IR,T}$ and $\omega_{IR,L}$ across different glasses, $\omega_{IR,T} = \omega_{BP}$ appears to hold consistently in 2D and 3D glasses.

First, we revisit the correlation between $\omega_{IR,T}$ and ω_{BP} in our studied 2D IPL-12 model glass formers in Figs. 2(a) and (b) and in 3D IPL-12 ones in Figs. 2(c) and (d). Note that Figs. 2, 3, and 4 are presented using a consistent plotting format for clarity. ω_{BP} is

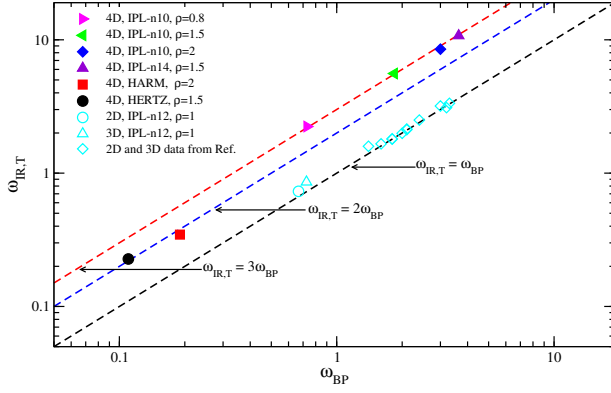


FIG. 5. Correlation between the boson peak frequency ω_{BP} and the transverse Ioffe-Regel limit frequency $\omega_{IR,T}$. Some 2D and 3D data shown here are from Ref. [43]. The values of ω_{BP} and $\omega_{IR,T}$ for each 4D system shown here are listed in Table. I

typically identified as the peak position in the reduced plot of $D(\omega)/\omega^{d-1}$ versus ω , as shown in Figs. 2 (a) and (c). $\omega_{IR,T}$ is determined by the intersection between the line representing $\Gamma_T(\omega) = \omega/\pi$ and the one representing the polynomial fit to the calculated $\Gamma_T(\omega)$ data, see Figs. 2 (b) and (d). One could observe that the vertical dashed line (representing $\omega_{IR,T}$) passing through Fig. 2(a) and (b) is located near the boson peak position (ω_{BP}) in Fig. 2(a), thus suggesting $\omega_{IR,T} \approx \omega_{BP}$. Similar results can be observed in Figs. 2 (c) and (d) for 3D glasses. Therefore, the previously reported equality $\omega_{IR,T} = \omega_{BP}$ is further supported by our studied 2D and 3D model glasses.

A compilation of simulation studies on 2D and 3D model structural glasses indicates that $\omega_{IR,T} = \omega_{BP}$. Then, it is natural to examine whether the relation $\omega_{IR,T} = \omega_{BP}$ still holds in higher spatial dimensional glasses. To the best of our knowledge, the correlation between $\omega_{IR,T}$ and ω_{BP} in systems with $d > 3$ has yet to be investigated, though there have been some studies of VDOS in such systems [63–66]. Here, we performed computer simulations to investigate their correlation in 4D model structural glasses with different types of interaction potentials and/or number densities.

We are now in a position to demonstrate our main findings in this work. We first show results in 4D IPL glasses. We compare $\omega_{IR,T}$ and ω_{BP} in 4D IPL-10 systems in Fig. 3. We show results from 4D IPL-10 systems at $\rho = 0.8$ in Figs. 3 (a) and (b); unexpectedly, one could observe that the vertical line representing $\omega_{IR,T}$ is far away from the position of the boson peak in Fig. 3 (a). This is very different from the observations from Fig. 2 for 2D and 3D glasses. The similar conclusion can be drawn from Figs. 3 (c) and (d) for 4D IPL-10 systems at $\rho = 1.5$. These observations in 4D IPL systems thus suggest that $\omega_{IR,T}$ appears at a higher frequency than ω_{BP} , which is our main finding in this work.

Additionally, our finding of $\omega_{IR,T} > \omega_{BP}$ is further

TABLE I. The boson peak frequency ω_{BP} , the transverse Ioffe-Regel limit frequency $\omega_{IR,T}$, and the number density ρ in 4D systems studied in this work. Here, ω_{BP} is determined as the peak position in the plot of $D(\omega)/\omega^3$ versus ω , whereas $\omega_{IR,T}$ is the intersection between the line representing $\Gamma_T(\omega) = \omega/\pi$ and the one representing the polynomial fit to the $\Gamma_T(\omega)$ data, as shown in Figs. 3 and 4.

System	ρ	ω_{BP}	$\omega_{IR,T}$
4D IPL-n10	0.8	0.73	2.24
4D IPL-n10	1.5	1.84	5.59
4D IPL-n10	2.0	3.00	8.51
4D IPL-n14	1.5	3.64	10.74
4D HARM	2.0	0.19	0.35
4D HERTZ	1.5	0.11	0.23

supported by results from 4D glasses with spring-like potentials. The studied systems with such potentials are 4D HARM glasses at $\rho = 2.0$ in Figs. 4 (a) and (b) and 4D HERTZ glasses at $\rho = 1.5$ in Figs. 4 (c) and (d). Apparently, the plots in Fig. 4 indicate that $\omega_{IR,T}$ is greater than ω_{BP} .

IV. CONCLUSION

In this work, we investigate the relation between the boson peak and the transverse Ioffe-Regel limit in 4D glasses. Our main finding is that the transverse Ioffe-Regel limit is reached at a much higher frequency than the boson peak frequency in all our studied 4D glasses. Specifically, Fig. 5 summarizes the relation between $\omega_{IR,T}$ and ω_{BP} in our studied 4D glasses as well as in previously studied 2D and 3D glasses [43]. If assuming $\omega_{IR,T} = A\omega_{BP}$, one could observe that $A \approx 1$ in 2D and 3D glasses. However, in 4D systems, we find $A \approx 2$ in HARM and HERTZ glasses, whereas $A \approx 3$ in IPL-10 and IPL-14 glasses. This indicates that $\omega_{IR,T} > \omega_{BP}$, and $\omega_{IR,T}$ is not proportional to ω_{BP} as the proportionality coefficient A is not constant. Note that the possibility that A may assume other values including unity, in other 4D glasses not examined here cannot be ruled out. Our current findings thus suggest that the previously proposed coincidence between the boson peak and the transverse Ioffe-Regel limit depends on spatial dimensions.

The reported coincidence between the transverse Ioffe-Regel limit and the boson peak frequency in 2D and 3D model structural glasses is believed to offer a unique perspective for understanding the origin of the boson peak [43]. However, it should be noted that a simulation study [20] of 2D mass-spring networks where specific types of disorder can be tuned artificially, suggested that the relation $\omega_{IR,T} = \omega_{BP}$ is conditional, as it demonstrated the possibility of observing $\omega_{IR,T} > \omega_{BP}$. We

also notice that the heterogeneous elasticity theory predicts the possibility of observing $\omega_{\text{IR},T} > \omega_{\text{BP}}$ under appropriate conditions [25]. However, such inequality has not been observed convincingly in any simulation study of more realistic model structural glasses where various types of disorder coexist. Additionally, our observation of $\omega_{\text{IR},T} > \omega_{\text{BP}}$ in 4D glasses in this work implies that it would be necessary to revisit whether $\omega_{\text{IR},T} > \omega_{\text{BP}}$ can also be observed in specific 2D or 3D model structural glasses.

ACKNOWLEDGMENTS

We acknowledge the support from National Natural Science Foundation of China (Grant Nos. 12522503 and 12374202), Anhui Projects (Grant Nos. 2022AH020009, S020218016 and Z010118169), and Hefei City (Grant No. Z020132009). We also acknowledge Hefei Advanced Computing Center, Beijing Super Cloud Computing Center, and the High-Performance Computing Platform of Anhui University for providing computing resources.

DATA AVAILABILITY

The data that support the findings of this study are available from the corresponding authors upon reasonable request

-
- [1] L. Berthier and G. Biroli, *Rev. Mod. Phys.* **83**, 587 (2011).
 - [2] E. Lerner and E. Bouchbinder, *J. Chem. Phys.* **155**, 200901 (2021).
 - [3] L. Wang, D. Xu, S. Zhang, Y. Nie, H. Tong, and N. Xu, *Rep. Prog. Phys.* **88**, 104601 (2025).
 - [4] R. C. Zeller and R. O. Pohl, *Phys. Rev. B* **4**, 2029 (1971).
 - [5] P. W. Anderson, B. I. Halperin, and C. M. Varma, *Philos. Mag.* **25**, 1 (1972).
 - [6] R. O. Pohl, X. Liu, and E. Thompson, *Rev. Mod. Phys.*, **74**, 991 (2002).
 - [7] M. A. Ramos, *Low-temperature thermal and vibrational properties of disordered solids* (Singapore, World Scientific, 2022).
 - [8] E. Flenner, L. Wang, and G. Szamel, *Soft Matter* **16**, 775 (2020).
 - [9] N. Xu, V. Vitelli, M. Wyart, A. J. Liu, and S. R. Nagel, *Phys. Rev. Lett.* **102**, 038001 (2009).
 - [10] C. Kittel, *Introduction to solid state physics*, 7th ed. (Wiley, New York, 1996).
 - [11] H. Mizuno, H. Shiba, and A. Ikeda, *Proc. Natl. Acad. Sci. U.S.A.* **114** E9767 (2017).
 - [12] L. Wang, A. Ninarello, P. Guan, L. Berthier, G. Szamel, and E. Flenner, *Nat. Commun.* **10**, 26 (2019).
 - [13] L. Wang, G. Szamel, and E. Flenner, *Phys. Rev. Lett.* **127**, 248001 (2021).
 - [14] N. Xu, V. Vitelli, A. J. Liu, and S. R. Nagel, *Europhys. Lett.* **90**, 56001 (2010).
 - [15] L. Wang, L. Fu, and Y. Nie, *J. Chem. Phys.* **157**, 074502 (2022).
 - [16] L. Wang, G. Szamel, and E. Flenner, *J. Chem. Phys.* **158**, 126101 (2023).
 - [17] E. Lerner, G. Düring, and E. Bouchbinder, *Phys. Rev. Lett.* **117**, 035501 (2016).
 - [18] L. Wang and N. Xu, *Phys. Rev. Lett.* **112**, 055701 (2014).
 - [19] Y. -C. Hu and H. Tanaka, *Nat. Phys.* **18**, 669 (2022).
 - [20] Y. Nie, H. Tong, J. Liu, M. Zu, and N. Xu, *Front. Phys.* **12**, 126301 (2017).
 - [21] W. Schirmacher, *Phys. Status Solidi B* **250**, 937 (2013).
 - [22] M. Baggioli and A. Zaccane, *Phys. Rev. Lett.* **122**, 145501 (2019).
 - [23] D. A. Parshin, H. R. Schober, and V. L. Gurevich, *Phys. Rev. B* **76**, 064206 (2007).
 - [24] B. Rufflé, D. A. Parshin, E. Courtens, and R. Vacher, *Phys. Rev. Lett.* **100**, 015501 (2008).
 - [25] W. Schirmacher, G. Ruocco, and T. Scopigno, *Phys. Rev. Lett.* **98**, 025501 (2007).
 - [26] S. Mahajan and M. P. Ciamarra *Phys. Rev. Lett.* **127**, 215504 (2021).
 - [27] G. Ding, E. Ma, F. Jiang, J. Duan, S. Cai, N. Xu, B. Cui, L. Dai, and M. Jiang, *Nat. Phys.* (2025). <https://doi.org/10.1038/s41567-025-03057-7>
 - [28] E. Flenner and G. Szamel, *Sci. Adv.* **11**, eadu6097 (2025).
 - [29] M. Shimada, H. Mizuno, and A. Ikeda, *Phys. Rev. E* **97**, 022609 (2018).
 - [30] S. Gelin, H. Tanaka, and A. Lemaitre, *Nat. Mater.* **15**, 1177 (2016).
 - [31] A. Moriel, G. Kapteijns, C. Rainone, J. Zylberg, E. Lerner, and E. Bouchbinder, *J. Chem. Phys.* **151**, 104503 (2019).
 - [32] L. Wang, L. Berthier, E. Flenner, P. Guan, and G. Szamel, *Soft Matter* **15**, 7018 (2019).
 - [33] L. Wang, G. Szamel, and E. Flenner, *Soft Matter* **16**, 7165 (2020).
 - [34] L. Fu and L. Wang, *Phys. Rev. E* **106**, 054605 (2022).
 - [35] L. Fu, Y. Zheng, and L. Wang, *Chin. Phys. B* **33**, 056401 (2024).
 - [36] G. Szamel and E. Flenner, *J. Chem. Phys.* **156**, 144502 (2022).
 - [37] G. Szamel and E. Flenner, *J. Chem. Phys.* **163**, 050903 (2025).
 - [38] G. Monaco and S. Mossa, *Proc. Natl. Acad. Sci. U. S. A.* **106**, 16907 (2009).
 - [39] A. F. Ioffe and A. R. Regel, *Prog. Semicond.* **4**, 237 (1960).
 - [40] S. N. Taraskin and S. R. Elliott, *Phys. Rev. B* **61**, 12031 (2000).
 - [41] D. A. Conyuh and Y. M. Beltukov, *Phys. Rev. B* **103**, 104204 (2021).
 - [42] Y. M. Beltukov, V. I. Kozub, and D. A. Parshin, *Phys. Rev. B* **87**, 134203 (2013).

- [43] H. Shintani and H. Tanaka, *Nat. Mater.* **7**, 870 (2008).
- [44] H. Mizuno, S. Mossa, and J. L. Barrat, *Proc. Natl. Acad. Sci. U. S. A.* **111**, 11949 (2014).
- [45] H. Mizuno and A. Ikeda, *Phys. Rev. E* **98**, 062612 (2018).
- [46] H. Mizuno, M. Hachiya, and A. Ikeda, *J. Chem. Phys.* **156**, 204505 (2022).
- [47] Y. M. Beltukov, C. Fusco, D. A. Parshin, and A. Tanguy, *Phys. Rev. E* **93**, 023006 (2016).
- [48] A. Marruzzo, W. Schirmacher, A. Fratalocchi, and G. Ruocco, *Sci. Rep.* **3**, 1407 (2013).
- [49] N. Jakse, A. Nassour, and A. Pasturel, *Phys. Rev. B* **85**, 174201 (2012).
- [50] Z. Liang and P. Keblinski, *Phys. Rev. B* **93**, 054205 (2016).
- [51] X. Wang, W. Zheng, L. Wang, and N. Xu, *Phys. Rev. Lett.* **114**, 035502 (2015).
- [52] J. Jiang and N. Xu, *Chin. J. Chem.* **40**, 1091 (2022).
- [53] B. Rufflé, G. Guimbretière, E. Courtens, R. Vacher, and G. Monaco, *Phys. Rev. Lett.* **96**, 045502 (2006).
- [54] G. Ruocco, A. Matic, T. Scopigno, and S. N. Yannopoulos, *Phys. Rev. Lett.* **98**, 079601 (2007).
- [55] T. Scopigno, J. -B. Suck, R. Angelini, F. Albergamo, and G. Ruocco, *Phys. Rev. Lett.* **96**, 135501 (2006).
- [56] E. Courtens, M. Foret, B. Rufflé, and R. Vacher, *Phys. Rev. Lett.* **98**, 079603 (2007).
- [57] B. Ruta, G. Baldi, F. Scarponi, D. Fioretto, V. M. Giordano, and G. Monaco, *J. Chem. Phys.* **137**, 214502 (2012).
- [58] M. Hassaine and M. A. Ramos, *Phys. Rev. B* **85**, 104206 (2012).
- [59] G. Baldi, V. M. Giordano, G. Monaco, and B. Ruta, *Phys. Rev. Lett.* **104**, 195501 (2010).
- [60] L. Wang, Y. Duan, and N. Xu, *Soft Matter* **8**, 11831 (2012).
- [61] E. Bitzek, P. Koskinen, F. Gähler, M. Moseler, and P. Gumbsch, *Phys. Rev. Lett.* **97**, 170201 (2006).
- [62] <https://software.intel.com/en-us/mkl/>
- [63] M. Shimada, H. Mizuno, L. Berthier, and A. Ikeda, *Phys. Rev. E* **101**, 052906 (2020).
- [64] P. Charbonneau, E. I. Corwin, G. Parisi, A. Poncet, and F. Zamponi, *Phys. Rev. Lett.* **117**, 045503 (2016).
- [65] L. Wang, D. Xu, and S. Zhang, *Chin. Phys. B* **33**, 076401 (2024).
- [66] G. Kapteijns, E. Bouchbinder, and E. Lerner, *Phys. Rev. Lett.* **121**, 055501 (2018).